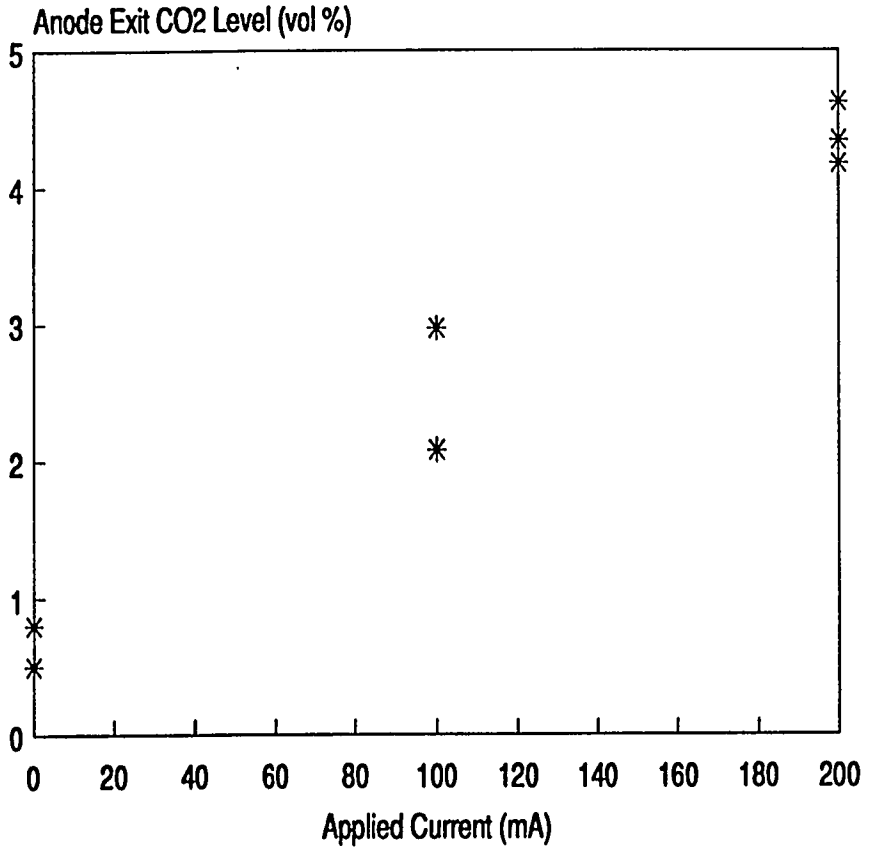

Inlet CO2 Level = 0 %
Anode Flow = 100 cc/min
Temp = 650 C

Figure 34 Run 34: Exit CO_2 Level vs Applied Current

Run 4

A rigid Zirconia mat worked in this experiment. The mat began as a weave of zirconia cloth, then hardened with the zirconia rigidizer, accomplished in a similar fashion as aforementioned. Housing materials were MACOR (machineable ceramic) with lithiated Ni electrodes and seals created from oxidation of aluminum. Seal formation created the opportunity to test carbonate transport through the E.M.S system with cathodic reduction (equation 7) and anodic reduction (equation 10) corresponding to 100% tranport with applied current. The temperature and flow rate were maintained at 650^{0}C and 215 cc/min respectively. Once efficient carbonate transport showed the system operable application of H_2S followed; inlet H_2S was held between 6 and 20 ppm H_2S. As much as 94% removal with applied current was seen in this experiment as shown. Exit H_2S and applied current vs potential difference (cathode to anode) are shown in figures 35 & 36. The results of both run 4 & 5 are tabulated in Table 4. The experiment was shut down due to hydrogen cross-over. Run #4 lasted 163 hours.

Cross-cell Potential vs H2S Removal

Run #4

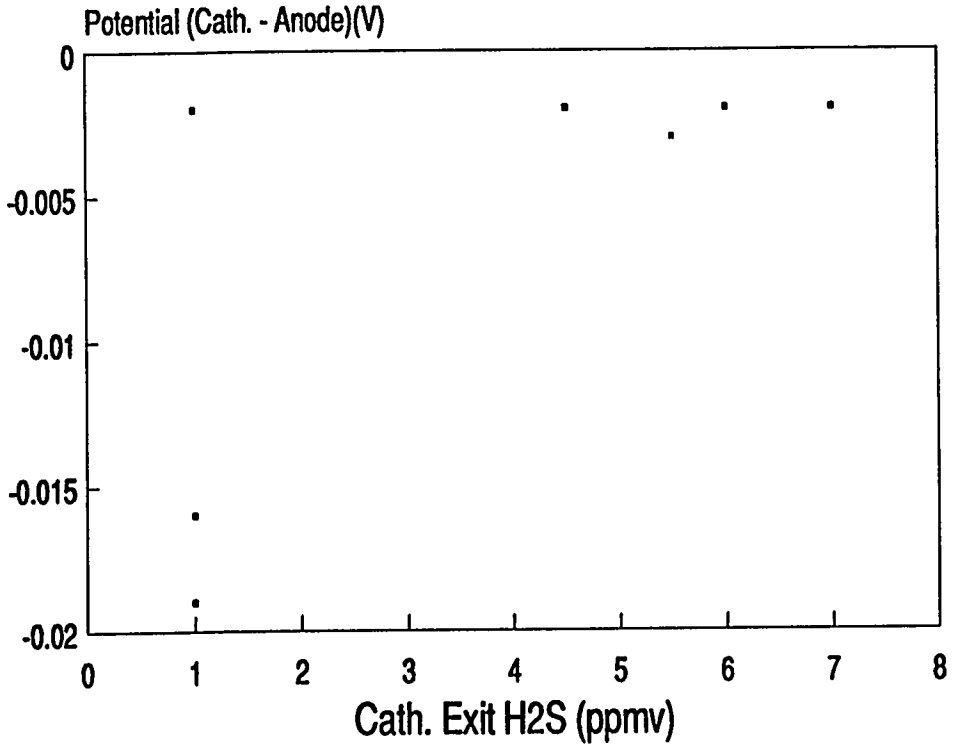

Temp. = 650 C
Flow Rate = 215 cc/min
Inlet H2S = 10 ppmv

Figure 35 Cross-cell Potential vs H_2S Removal

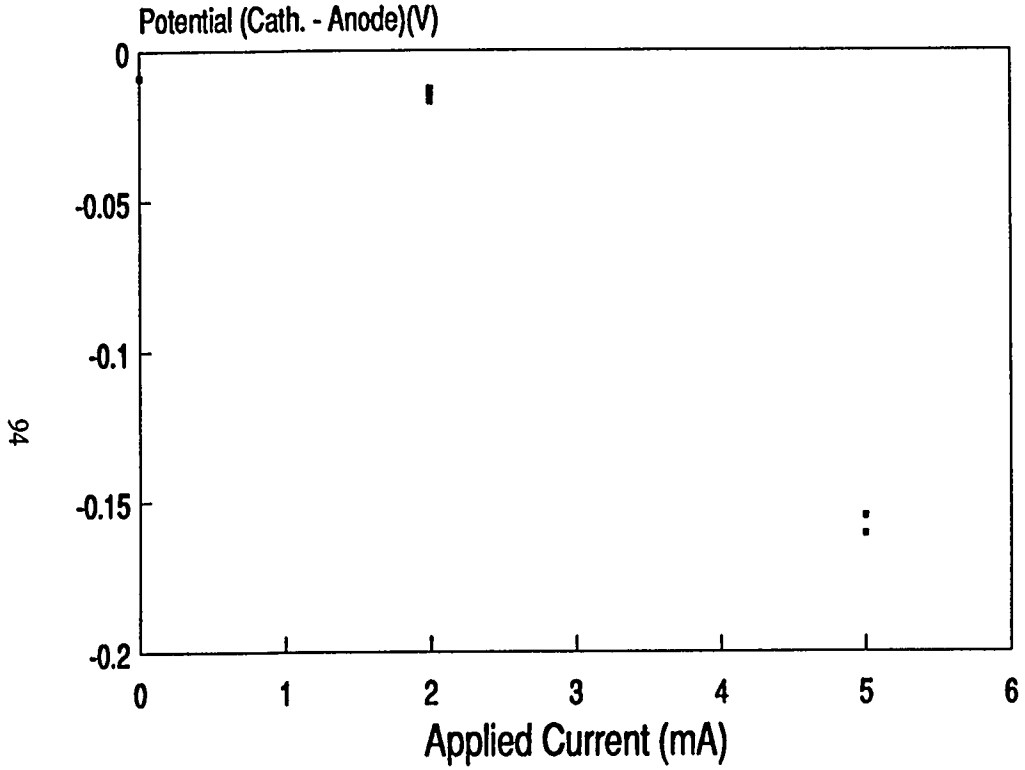

Figure 36 Cross-cell Potential vs Applied Current

Run 5

A manufactured Zircar membrane provided the medium for electrolyte support. Other materials were identical to Run 4. The manufactured membrane is advantagous, due to uniform porosity (66%) and reduced warping. Once efficient carbonate transport occurred, H_2S was applied to the cell and held at a concentration of 20 ppm. Flow rates varied from 200 cc/min - 800 cc/min at constant temperature (650° C). Removals over 90% were recorded with applied current. Exit H_2S and applied current vs cross-cell potential (cathode-anode) are shown in figures 37 & 38. The cell was shut down after 208 hours, due to an increase in membrane thickness, limiting sulfide migration.

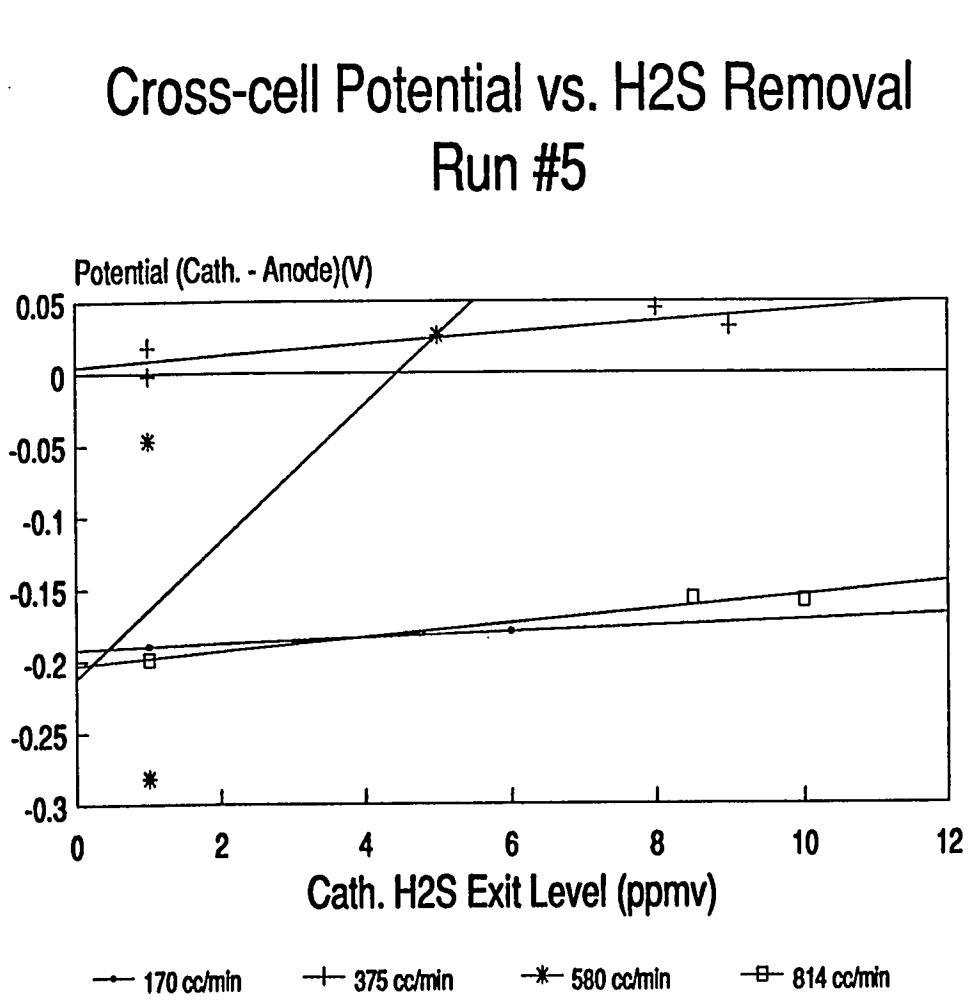

Inlet H2S = 20 ppmv
Temp. = 650 C

Figure 37 Cross-cell Potential vs H_2S Removal

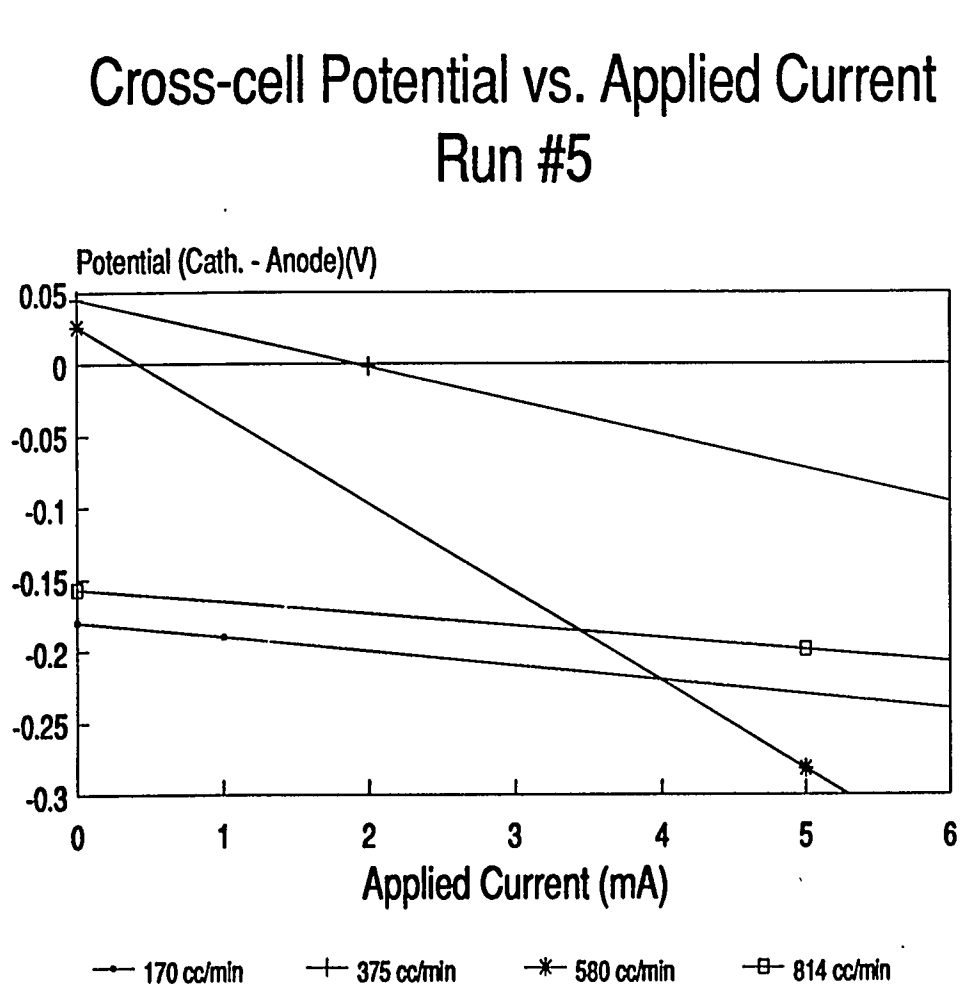

Inlet H2S = 20 ppmv
Temp. = 650 C

Figure 38 Cross-cell Potential vs Applied Current

Table IV. Experimental Results for Runs #4 & #5

Temp. (°C)	Flow-Rate (cc/min)	Residence Time (sec.)	Inlet H_2S (ppm)	Exit H_2S (@ I_{app})	I_{app} (mA)	E_{c-a} (Volts)
650	170	0.197	25	1	1	-0.190
	225	0.146	8.5	1	2	-0.013
	375	0.089	22	1	2	-0.003
	580	0.058	20	1	5	-0.047
	814	0.041	22	1	5	-0.199

CONCLUSIONS

The most important issue facing the removal of H_2S by the Electrochemical Membrane Separator is finding/developing an adequate matrix material that simultaneously sustains an ionic pathway and hinders process-gas cross-over. Exploration of various matrix materials and manufacturing techniques revealed a variety of possibilities for the electrochemical separation cell; matrices of densified zirconia provided the best results in full-cell experimentation.

Anodes of lithiated Ni converted to NiO in-situ performed effectively with similar usefulness at the cathode; however, H_2S levels > 100 ppm requires an alternate cathode material due to the conversion of NiO to a molten nickel sulfide. Recent experiments using cobalt cathodes have been successful.

High temperature removal of over 90% H_2S utilized the aforementioned membrane and electrode materials attaining the removals with high current efficiencies and low polarizations, creating a low overall power requirement.

SO_2 REMOVAL

SO_2 removal is carried out through electrochemical steps, in combination with a number of chemical steps. The overall reaction involves the selective removal of SO_x from the cathodic (reducing) side of the membrane, and the generation of SO_3 and some O_2 at the anodic (oxidizing) side. This SO_3 and oxygen can be concentrated to produce a stream for use in production of a high purity oleum. This reaction takes place over a molten salt electrolyte consisting of 90 wt% $K_2S_2O_7$ and 10 wt% V_2O_5 at 400° C.

The chemical reactions of $K_2S_2O_7$ melts over varying temperatures were analyzed by Flood *et. al.*[20,21]. Their experiments, carried out with SO_3, SO_2, and O_2, determined that two chemical equilibriums existed. The first was an equilibrium imposed with SO_3:

$$M_2SO_4 + SO_3 \rightleftharpoons M_2S_2O_7 \qquad (37)$$

with stability of the melt being the highest when M=K. The second equilibrium of importance was with SO_2 and O_2 present:

$$SO_2 + \tfrac{1}{2}O_2 + K_2SO_4 \rightleftharpoons K_2S_2O_7 \qquad (38)$$

Flood then made an estimation for the ratio of liquidus activity coefficients based upon variations from Nernstian effects in electrolyte of known composition and at constant temperature and partial pressures. There is suggestion of an eutectic melt at approximately 400° C, with a sulfate solubility of approximately 3-5wt% in pyrosulfate.

Boreskov *et. a.*[22] further attempted to study $K_2S_2O_7$ in conjunction with V_2O_5 under oxygen at various temperatures, but could not decipher the reactions from 400-500° C. He did, however, suspect the formation of a $K_2S_2O_7$-V_2O_5 compound.

Fang and Rapp *et. al.*[23,24,25] found that at a platinum electrode at 900° C, pyrosulfate reduction in a sulfate melt would require one electron, and be reduced according to:

$$S_2O_7^{2-} + e^- \rightleftharpoons SO_4^{2-} + SO_3^- \qquad (39)$$

The SO_3^- ion would not be stable in the melt, and could react with itself to form the bisulfite ion, or with one electron, to form the sulfite ion. They further determined that neither the sulfite nor bisulfite ions would be stable in the melt, but would chemically react as

$$S_2O_6^{2-} \rightleftharpoons 2SO_2 + O_2^{2-} \qquad (40)$$

and

$$SO_3^{2-} \rightleftharpoons SO_2 + O^{2-} \qquad (41)$$

Franke[26] and Scott[27] completely decoded the reactions in the electrolyte through use of techniques including cyclic voltammetry, equilibrium potential techniques, X-ray diffraction, and effluent analysis. Performed upon potassium pyrosulfate ($K_2S_2O_7$) with variations in the gas composition as well as the salt itself, their analysis determined the dominant reactions.

Simulated exit gas is first introduced ex-situ to Pt or an acid catalyst such as Haldor-Topsoe VK-38 where all SO_2 is converted to SO_3 according to

$$\text{(42)} \quad SO_2 + \tfrac{1}{2}O_2 \rightarrow SO_3$$

This SO_3 stream enters the cell, and is then passed over the cathodic side of the cell as seen in Figure 39.

Two electrons are supplied to the cathode to reduce pyrosulfate according to

$$2S_2O_7^{2-} + 2e^- \rightarrow 2SO_2 + 2SO_4^{2-} + O_2^{2-} \qquad (43)$$

It is important to note that the reduction of pyrosulfate involves the *production* of two moles SO_2. SO_2 present can react with the superoxide ion to generate the sulfite ion:

$$SO_2 + O_2^{2-} \rightarrow SO_4^{2-} \qquad (44)$$

SO_2 may also combine with the sulfate ion, forming the unstable bisulfate ion. Bisulfate will then rapidly decompose to form sulfur trioxide and the sulfite ion:

$$2SO_2 + 2SO_4^{2-} \rightarrow 2S_2O_6^{2-} \rightarrow 2SO_3 + 2SO_3^{2-} \qquad (45)$$

Sulfite ion, unstable in the melt, reacts with any dissolved oxygen in the system:

$$2SO_3^{2-} + O_2 \rightarrow 2SO_4^{2-} \qquad (46)$$

The SO_3, flowing over the cathodic surface, will react with sulfate ions present to reform the favored pyrosulfate ion according to:

$$2SO_3 + 2SO_4^{2-} \rightleftharpoons 2S_2O_7^{2-} \qquad (47)$$

If the preoxidation reaction of Equation (42) is considered, the summation of the reactions leaves the overall cathodic reaction as:

$$SO_2 + O_2 + 2e^- \rightarrow SO_4^{2-} \quad (48)$$

This reaction was confirmed by Townley[28] to remove one mole of SO_2 for every two electrons supplied. Salzano and Newman[29] demonstrated that a similar equilibrium could exist:

$$SO_3 + \tfrac{1}{2}O_2 + 2e^- \rightarrow SO_4^{2-} \quad (49)$$

Equation (49) is the sum of the above reactions without the preoxidation reactor taken into account and will be more indicative of the physical electrochemical cell, and the measurements thereof.

At the anode, the thermodynamically favored oxidation of the sulfate ion will take place according to:

$$SO_4^{2-} \rightarrow 2e^- + \tfrac{1}{2}O_2 + SO_3 \quad (50)$$

The sum of Equations (49) and (50) yield the overall cell reaction for the removal of SO_3 as:

$$(SO_3 + \tfrac{1}{2}O_2)_{cathode} \rightarrow (SO_3 + \tfrac{1}{2}O_2)_{anode} \quad (51)$$

The potential, if calculated from a cathodic stream of 3000 ppm SO_3 and 3.0 mole% O_2 concentrated to a stream of 66.7 mol% SO_3 and 33.3 mole% O_2 would be -192 mV at 400° C.

Two reactions of importance are the sum of Equations (45) and (46), and the chemical equilibrium of Equation (47). Summing the reactions yields the overall step in Equation (52). This step is catalyzed in situ by V_2O_5 present in the $K_2S_2O_7$ in

$$SO_2 + \frac{1}{2}O_2 \rightarrow SO_3 \qquad (52)$$

quantities up to 10 wt.%. V_2O_5 is used often as a catalytic oxidant for sulfuric acid production in oxygenated systems. Flood and Kleppa[30] studied the equilibrium reaction of SO_2/SO_3 over vanadia. They found evidence of vanadia complexing when characterizing the reaction. Maximum catalytic effect was found to take place at 530° C, the decomposition temperature of $VOSO_4$.

Franke found that the addition of V_2O_5 to the melt resulted in a two-step chemical oxidation:

$$2SO_2 + 2\,[K_2O\text{-}V_2O_5\text{-}2SO_3] \rightleftharpoons 2\,[K_2O\text{-}V_2O_4\text{-}3SO_3] \qquad (53)$$

$$O_2 + 2\,[K_2O\text{-}V_2O_4\text{-}3SO_3] \rightleftharpoons 2\,[K_2O\text{-}V_2O_5\text{-}2SO_3] + 2SO_3 \qquad (54)$$

The vanadia complex may also take part in either the storing of excess SO_3

$$[K_2O\text{-}V_2O_5\text{-}2SO_3] + 2SO_3 \rightleftharpoons [K_2O\text{-}V_2O_5\text{-}4SO_3] \qquad (55)$$

or an electrochemical reaction

$$[K_2O\text{-}V_2O_5\text{-}4SO_3] + 2e^- \rightleftharpoons [K_2O\text{-}V_2O_4\text{-}3SO_3] + SO_4^{2-} \qquad (56)$$

Karydis *et. al.*[31,32] studied the equilibrium chemistry of $V_2O_5/K_2S_2O_7$ in $SO_3/SO_2/N_2$ atmospheres, and concluded that an equilibrium existed as

$$(VO)_2O(SO_4)_2^{4-} + SO_2 \rightleftharpoons 2VO(SO_4)_2^{2-} + SO_3 \qquad (57)$$

Estimation of liquid and solid temperatures led to the construction of a phase diagram for low loadings of V_2O_5 in pyrosulfate.

The chemical equilibrium established in Equation (47) shows the dependence of the concentration of sulfate in the melt on the partial pressure of SO_3 over the melt. At just over 400° C, the equilibrium will be established between sulfate and pyrosulfate. At 400° C, however, there is a limited solubility of sulfate in pyrosulfate of 4 wt%.

The removal is accompished through the use of a ceramic matrix sandwiched by two porous gas diffusion electrodes, and impregnated with a molten salt electrolyte. As seen in Figure 40. The housings are constructed of 316LSS, with the electrode area encompasing approximately 20 cm^2 and membrane diameters of 7.62 cm. The 316LSS housings form a passivating layer, while still allowing current flow to the surface of the imbeded electrodes.

In accordance with the goals of the research, electrode and matrix materials were tested for performance and stability in this complicated system. This work and additional work with the electrolyte over the research period is detailed, followed by the resulting full cell tests of the integrated system.

Electrochemical Flue Gas Clean-Up

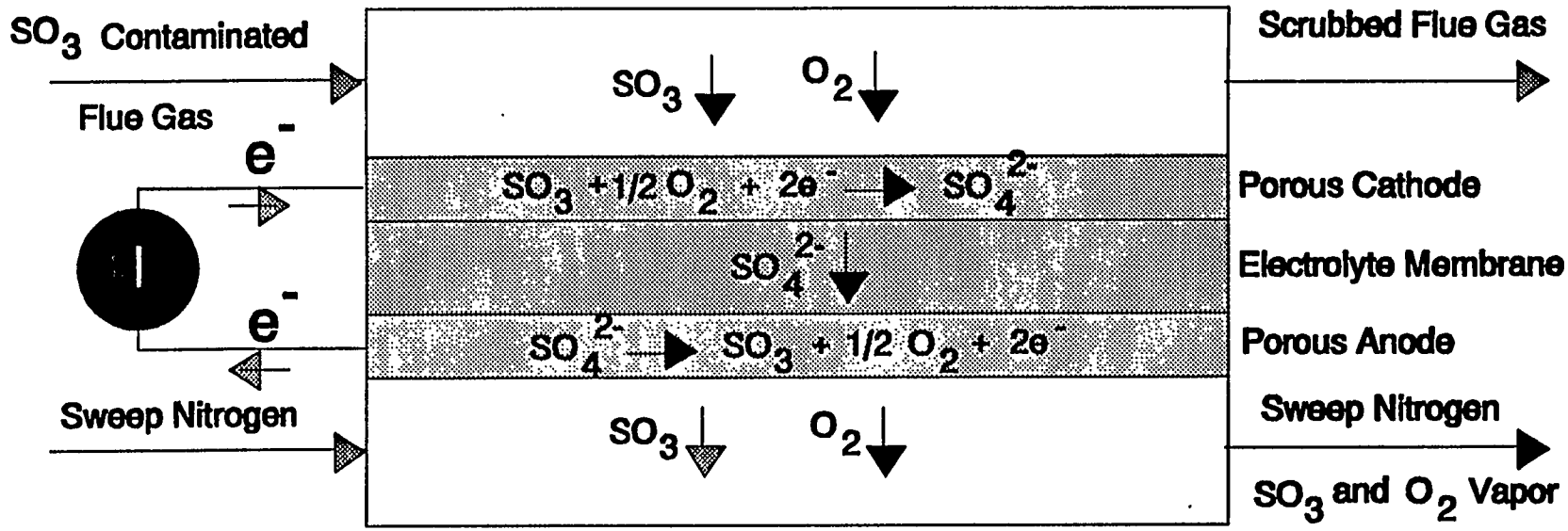

Figure 39: Conceptual cell configuration. T=400° C.

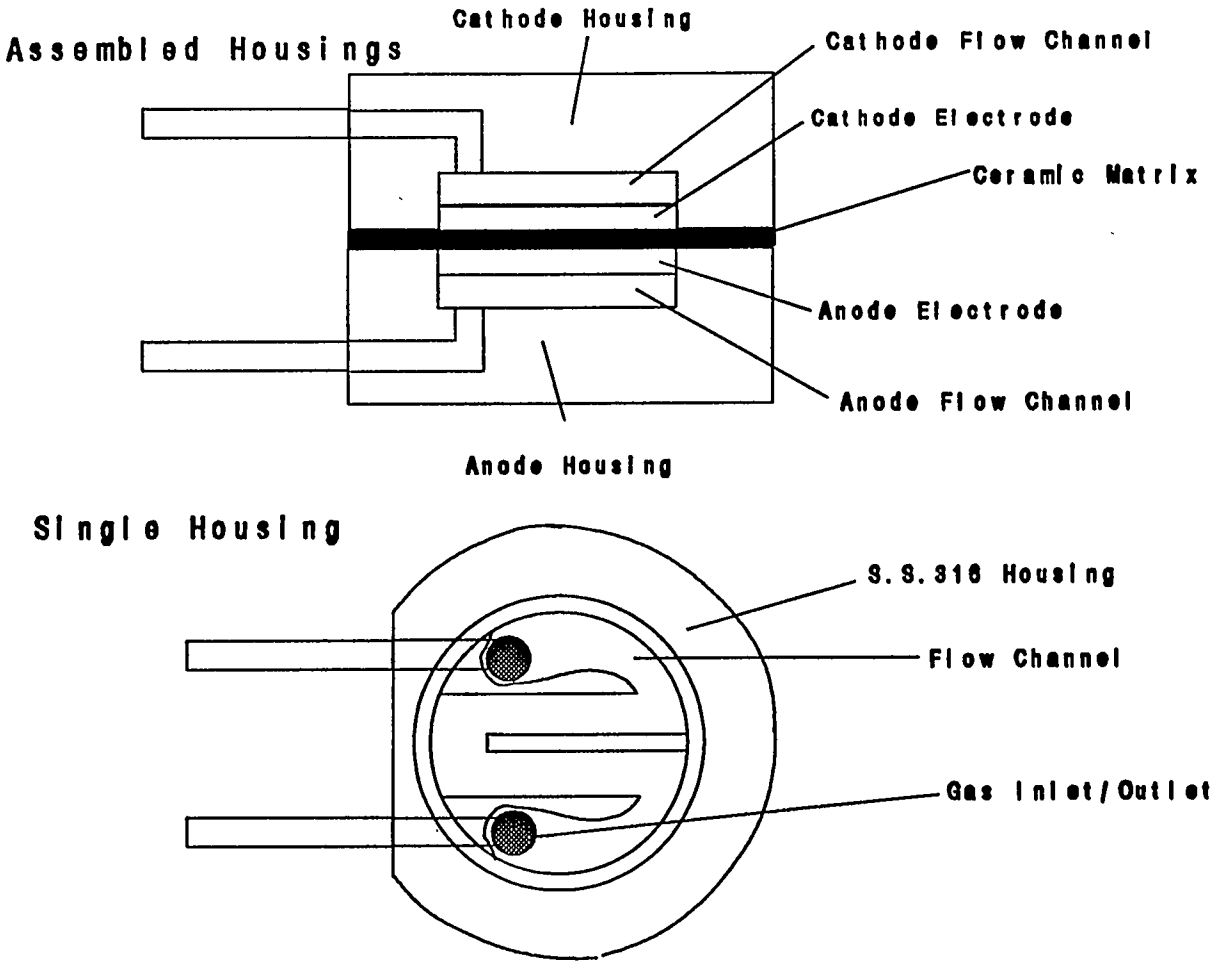

Figure 40: Bench scale full system test apparatus.

MATERIALS

There are a number of factors crucial to component development addressed throughout the following research. The first is the question of chemical and electrochemical stability. If either one of these tests if failed, the component will most certainly degrade, affecting total cell performance. Another aspect is the ability of the materials to be formed into the correct geometry. Costly material handling processes would negate the commercial viability of the system.

A last important factor is that of pore size matching between the porous electrode and the ceramic matrix. Impregnated electrolyte must be maintained in the ceramic matrix through capillary action, while still wetting the pores of the gas-diffusion electrode (see Figure 41). If the pores of the electrode are small enough to pull electrolyte from the matrix through capillary action, current and ion migration paths will be disrupted, as well as possible destruction of the wet seal formed by the matrix when wet with electrolyte. In addition, with electrolyte now flooding the porous electrode, the great advantage of increased transfer area will be lost as a smaller surface is presented to the gas flowing past the electrode, resulting in decaying performance.

These factors were kept in mind as the components of the full cell removal system were tested.

Electrodes

Many metals were investigated as electrodes, including stainless steels (SS 304, 347 and 430), oxidation-resistant alloys (Haynes 188 and Hastelloy-X) and nickel or lithiated nickel oxide. These materials were tested because they are commercially available in fibrous mesh form. Testing included cyclic voltammetry (CV) for corrosion resistance in the molten pyrosulfate ($K_2S_2O_7$) and longer duration stability tests, where samples were exposed to the molten salt and weight changes determined. The lithiated nickel oxide (a common molten carbonate fuel cell cathode material) was manufactured by soaking nickel mesh in 1M LiOH and heating to 600° C to form the lithiated nickel oxide. This structure was confirmed by X-ray powder diffraction, with the remaining phase being unoxidized nickel.

Of all the materials examined, lithiated nickel oxide appears to be the best. A CV on clean nickel wire showed a distinct oxidation peak, corresponding to the formation of NiO. After testing, the wire had gained an oxide coating on the area exposed to the melt. A CV on lithiated NiO mesh showed no oxidation peak. This test showed the electrochemical corrosion did not occur, but gave no conclusions as to chemical corrosion. Stability tests showed the formation of small amounts of $NiSO_4$, a corrosion product. This product is non-conductive, but no decrease in performance was seen during CVs and full cell tests (described below). The sulfates may be due to corrosion of either NiO or exposed Ni surfaces. Further evaluation continues on lithiated nickel oxide, but its polarization performance, with any membrane structure, is much better than the previously used perovskite electrodes, $La_{0.8}Sr_{0.2}CoO_3$ or $La_{0.8}Sr_{0.2}CuO_3$. Much of this improvement is due to the higher porosity (95%) and lower surface area

enhancement (actual = 12x superficial) compared with the perovskites (55% porous, 200x surface area enhancement). These factors reduce the possibility of electrode pore flooding.

Constant-current experiments with sufficient gas flow showed that the $La_{0.8}Sr_{0.2}CuO_3$, as an anode, decreases in polarization performance over time, whereas the lithiated NiO maintains, if not improves, its polarization performance. (Compare Figure 42 and Figure 43). After these experiments, the current polarity was switched, making the NiO the anode and the Cu-based perovskite the cathode. Figure 44 shows that the lithiated NiO electrode performs much better than the Cu-based perovskite as a cathode. Even as an anode, the lithiated NiO performs well.

It has been surmised by past researchers that the doping of the NiO lattice with the Li^+ ion results in a p-type semiconductor according to the Equation (58), which utilizes Kröger-Vink notation.

$$Li^{+} \rightarrow Li_{Ni}' + V_O^{\bullet\bullet} \qquad (58)$$

The equation shows that the proposed Li doped NiO lattice would conduct via holes, making it a p-type semi-conductor. This semiconductor should have the property of increasing conductivity with increasing temperature. It has been suggested, however, that the actual mechanism of conduction in the material is polaron conduction. This proposed type of conduction occurs when ions of the same type, but with valences differing by one, occupy adjacent lattice sites. The application of energy allows the change in valence of these adjacent states. In this case, the Ni ion may would be

present, after doping, in the Ni^{+2} and Ni^{+3} state within the lattice. The Ni^{+3} would exist to offset the charge imbalance imposed by the doping of the lattice with the Li^{+1} ion. Thermal excitation would allow the transfer of electrons from the Ni^{+2} ions to the Ni^{+3} ions. The concentration of carriers is dependant only upon the dopant level in the NiO, but the mobility of the electrons is dependant on the temperature and activation energy. A polaron-conducting material will thus show a similar dependance to temperature as a p-type or n-type semiconductor. In addition, the doping level for polarons will tend to be on the order of percent levels, whereas the doping level for a semiconductor can be on the order of parts per million. The formula for the doping of NiO with Li would be $Li_xNi_{1-x}O$.

Two lithiated NiO materials were studied; a proprietary nickel electrode from Energy Research Corporation (ERC) and a nickel mesh from National Standard (Fibrex). The Fibrex material is a sintered mesh of nickel fibers, each 25 microns nominal diameter, with powdered nickel carbonyl added to increase the structural strength of the bonds. The mesh is available in a variety of powder loadings, which has the effect of reducing the porosity of the mesh, while increasing the exposed surface area. The ERC electrode is a sintered nickel body made from particle precursors, producing an electrode with small pores. Since this material is proprietary in nature, only the relative effects of electrolyte wetting will be discussed.

National Standard Fibrex nickel electrodes were analyzed with X-ray powder diffraction to confirm the phases present after oxidation and exposure to electrolyte. After oxidizing the Ni electrodes in air at 600° C for 24 hours, the only NiO (Bunsenite)

was observed. A piece of lithiated NiO was treated in $K_2S_2O_7$ for 24 hours to determine chemical stability. The major phases were $LiNiO_2$ and NiO, with some $K_2Ni_2(SO_4)_3$. The $K_2Ni_2(SO_4)_3$ is a reaction product, most likely caused by reaction with exposed Ni on the surface. When the NiO is formed, the material goes through a 19% volume expansion (119% original size). Since the metal and the oxide have different thermal expansions, it is possible that cracks form in the oxide surface upon cooling, creating bare Ni surfaces prone to attack by $K_2S_2O_7$. X-ray powder diffraction analysis of used lithiated NiO electrodes was conducted. There were several phases present, predominately $LiNiO_2$, with some NiO and $K_2Ni_2(SO_4)_3$. The sulfate phase was present in approximately the same proportion as found in the stability tests mentioned above. No significant decrease in conductivity was found at the end of the run, even though non-conductive sulfates were present. It is unclear whether the sulfates result from corrosion of exposed Ni or SO_3 attack of NiO. The thermal expansion coefficients of Ni and NiO are very different, so that upon heating, some of the NiO may have separated, leaving Ni fibers exposed.

Ni electrodes from the Energy Research Corporation (ERC) were also tested. This proprietary material was lithiated and oxidized, at different temperatures, to determine the effect of oxidation temperature on room temperature conductivity (see Table V). At the lower temperatures, the surface exposed to air was darker than the underside, showing a possible limitation towards oxidation. All samples warped, due to either residual stress relief during heating or a loss of ductility in the oxidized area. The room

temperature resistances are tabulated below and show a strong dependence on firing temperature. All electrodes used in full cell tests were prepared at 575° C.

After electrode chemical stability tests proved successful, research progressed to characterize the surface and its interaction with the molten electrolyte. Figure 45 shows two scanning electron micrographs of the electrode material after its use in a full cell study. The electrode material is in the lithiated and oxidized state. The micrograph on the left displays the surface exposed to gas after use. The other micrograph exhibits the same surface after the electrode has been thoroughly washed. The effect of washing shows these electrodes to retain a large amount of electrolyte in the micropores, a symptom of electrode flooding. Many of the larger pores which run throughout the electrode are filled with electrolyte, reducing the surface area available for the removal of gaseous species. These SEMs confirm the behavior of the full cell during the run.

Figure 46 displays two SEMs of the raw mesh (50% fiber, 50% powder and 86% porous) at two different magnifications. The scan on the left, at 40x, shows the network of fibers with the powder covering the majority of the surface and providing an extensive network of macropores. The SEM on the right, at 3000x, provides a closer look at the micropores in the structure. The smooth nodules of nickel powder supply pores in the range of 1 to 10 microns, with very open gas flow passages between the micropores.

After treatment with LiOH, drying and subsequent oxidation of the Fibrex mesh, the surface of the nodules becomes coarse and the average pore size shrinks by about 20%. This shrinkage is caused by an expansion of the nickel as oxidation occurs (+19%

volume change from Ni to NiO). Figure 47 shows the pores to range from 1 to 7 microns.

Porosity experiments were then performed on five samples of both Fibrex and ERC electrodes, according to ASTM Standard Designation C 373-72. The results of the Fibrex electrodes are shown in Figure 49, along with the formulae used. The electrodes were heated to 150° C for 30 minutes to obtain the dry weight, boiled in water for 5 hours and then let sit overnight to obtain 25° C water. The saturated specimens were then carefully weighed, according to the standard, to obtain the saturated and suspended weights. These numbers are accurate to within 2%.

Mercury intrusion porosimetry was performed on the ERC and Fibrex electrode materials. The details of the ERC material will not be shown. A plot of volume % v. pore radius, Figure 50, shows that the vast majority (87%) of the pores are greater than 1 micron in diameter ($r = 0.55\mu$). Some of compiled data, Table VI, also showed that 57% of the pores were $\geq 4\ \mu$ in diameter, resulting in a good match with the electrolyte membrane structure.

Finally, the electrode resistance was measured while the electrode was subjected to temperature cycling. The electrode was attached to gold and platinum leads on either side, and the resistance between these leads measured. Corrections were made for the resistance of the leads, but not for the subsequent oxidation of the alligator clips used. It can be seen in Figure 51 that there is an initial large drop in resistance with increasing temperature. This is believed to be the effect of incomplete lithiation, with completion occurring in the first cycle. The resistance then follows the same curve, but tends to rise

slightly. This is believed to be the effect of oxidation of the stainless steel alligator clips used in connection. P-type semiconducting behavior is exhibited, with a resistance of approximately 1 Ω at 400° C.

Table V: Variation of lithiated NiO resistance with firing temperature and time.

Firing Temperature, and Time	Upper Surface Resistance (Room T)	Lower Surface Resistance (Room T)
500° C; 24 hrs.	220 Ω	1770 Ω
550° C; 12 hrs.	145 Ω	600 Ω
600° C; 2 hrs.	5 - 10 Ω	4 - 10 Ω
600° C; 2 hrs.	7 - 16 Ω	1.4 - 3 Ω

Table VI. Data for Mercury Porosimetry of Fibrex 50/50 mat.

Pore Radius, μm	Pore Diameter, μm	Intruded Volume, cc/g	% Volume Intruded
4.727	9.454	0.0139	3.8
1.947	3.894	0.2069	56.63
1.241	2.482	0.2579	70.58
0.8944	1.7888	0.2883	78.89
0.6942	1.3884	0.3052	83.52
0.5546	1.1092	0.3177	86.93
0.4554	0.9108	0.3264	89.33
0.3878	0.7756	0.3319	90.84

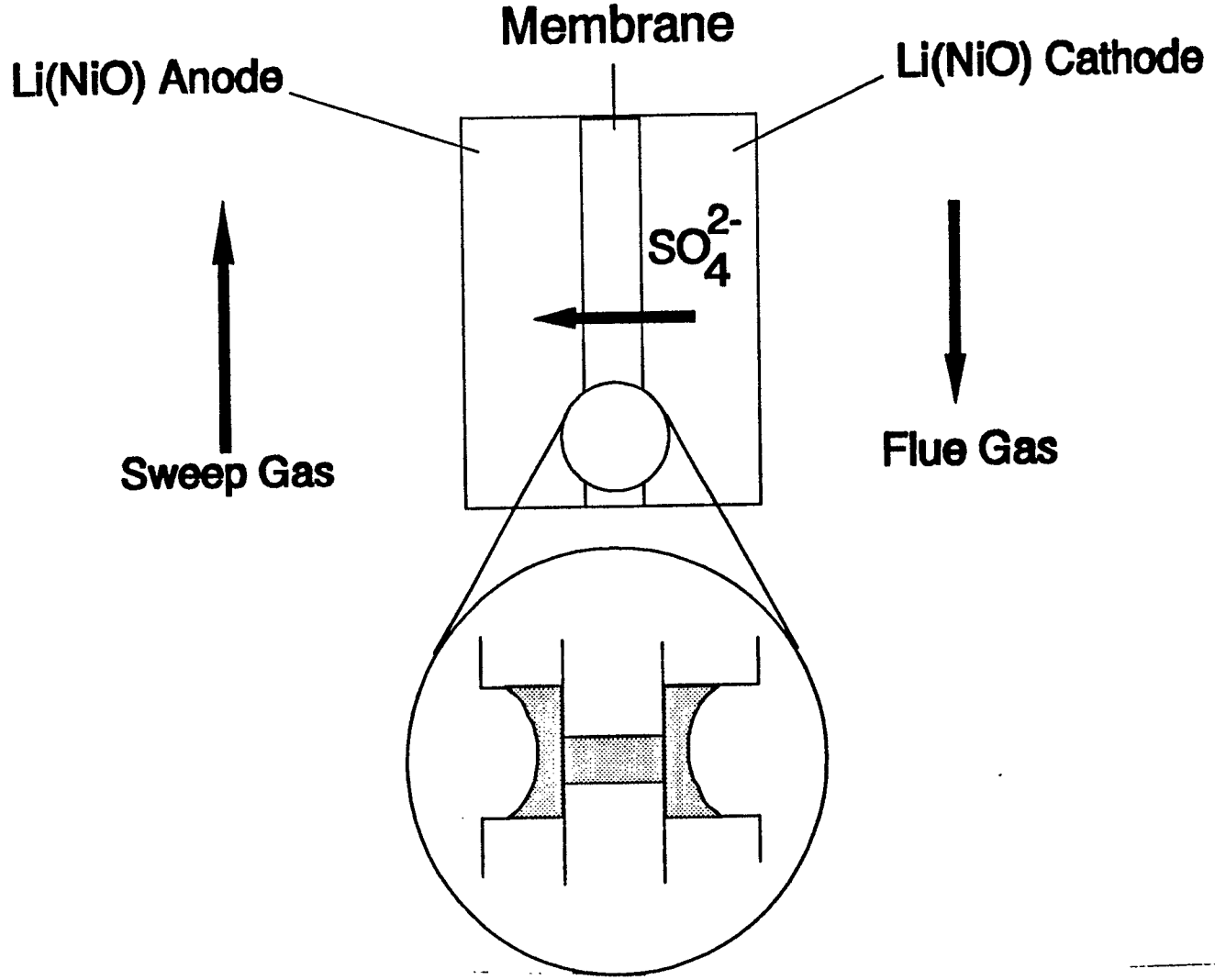

Figure 41: Pore wetting model desired in full cell removal systems.

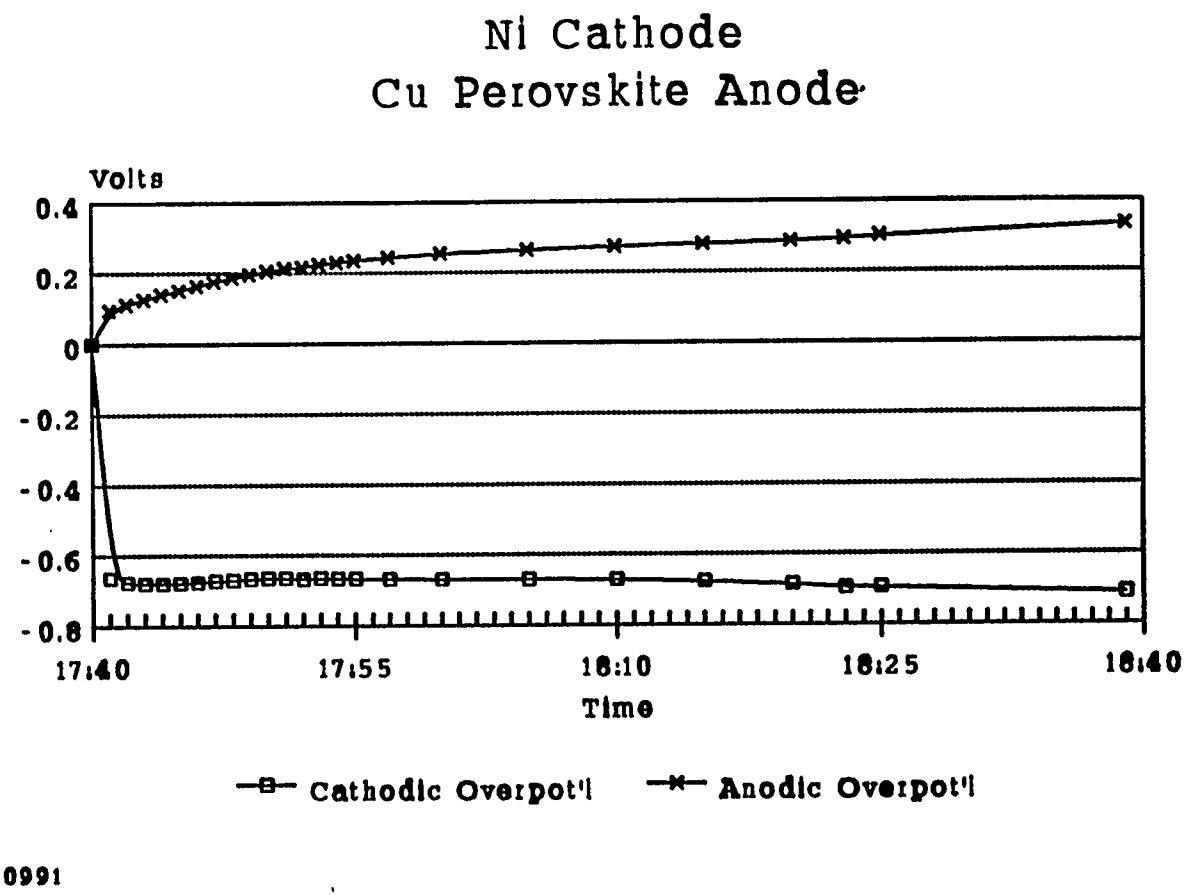

Figure 42. Cell electrode overpotentials at 400° C, 10 mA.

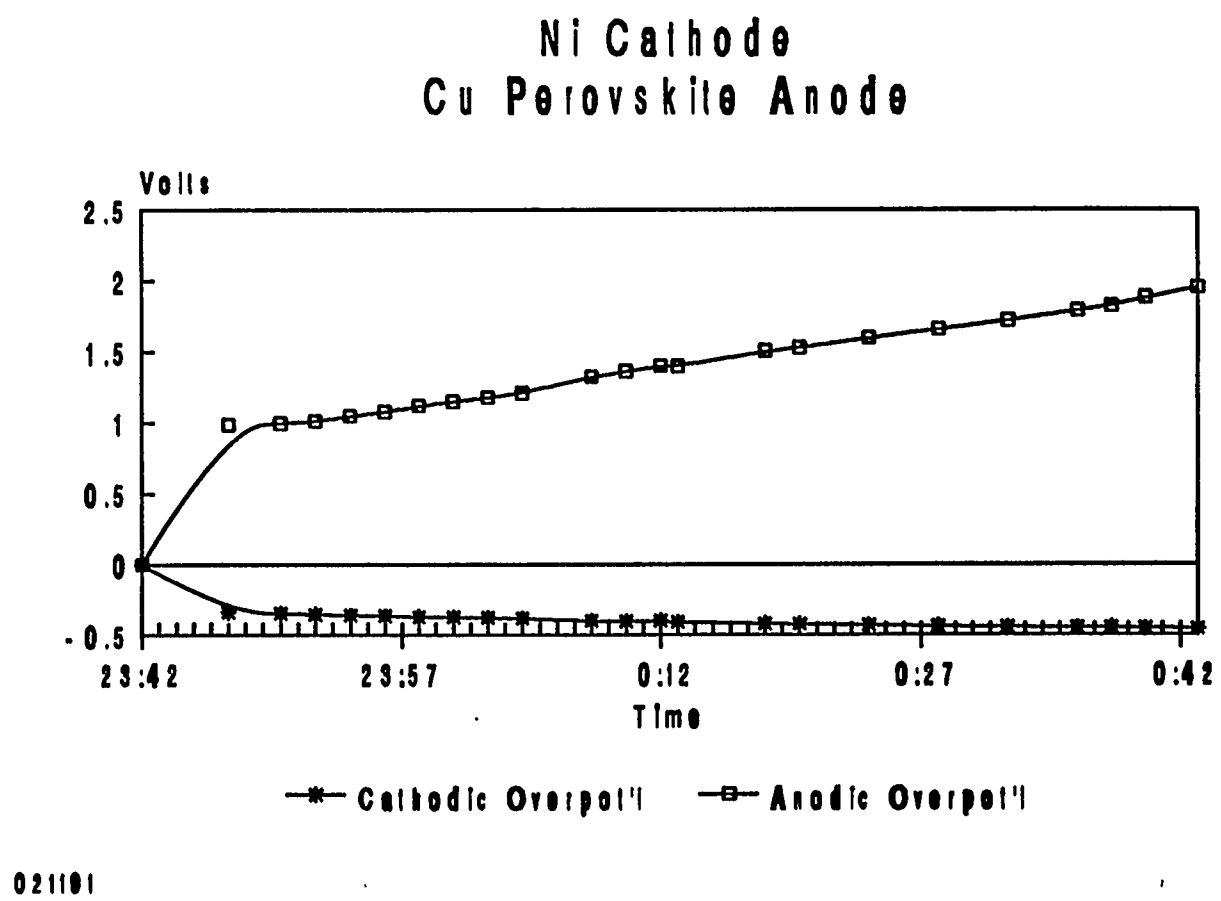

Figure 43. Cell electrode overpotentials at 400° C, 10 mA.

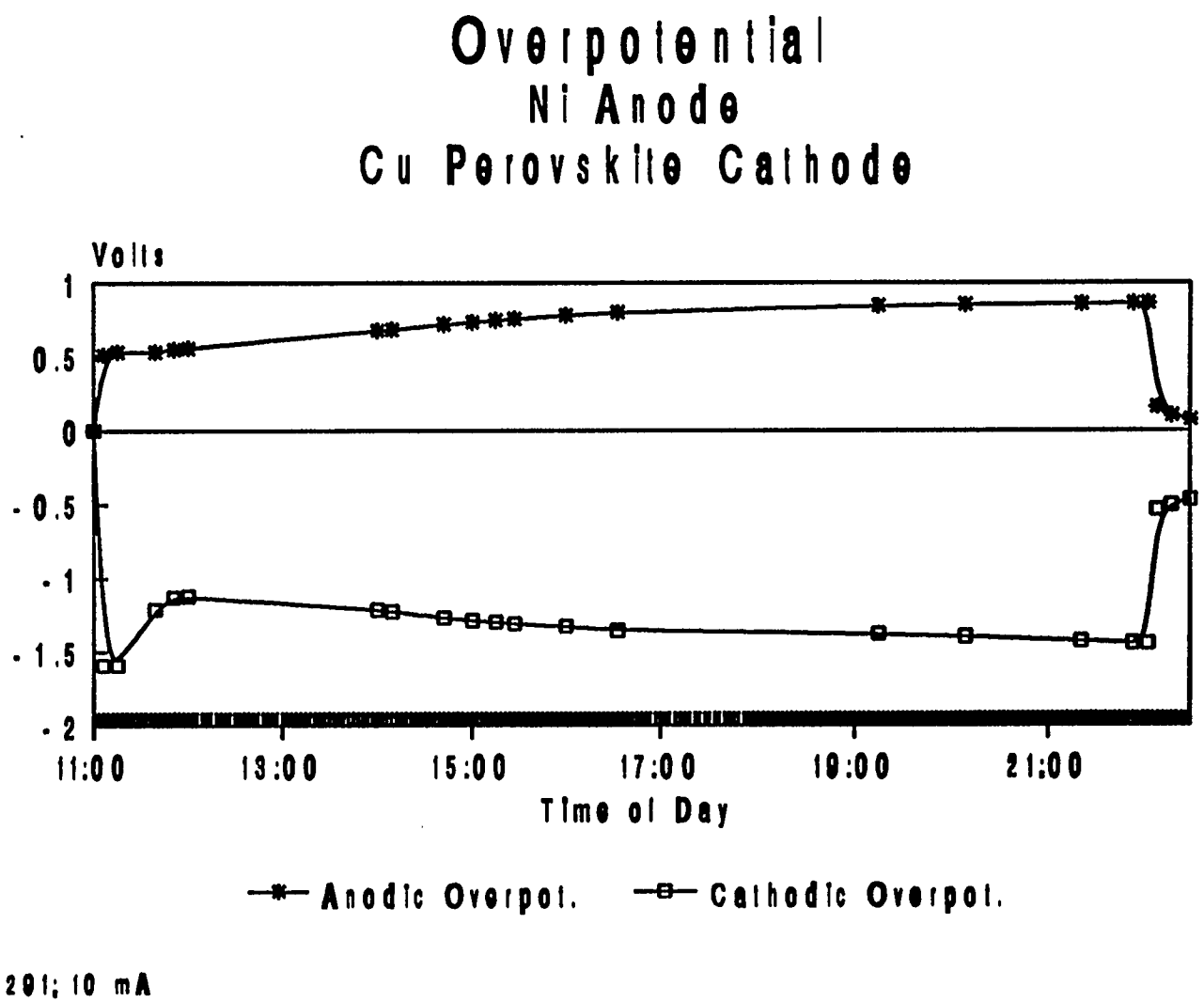

Figure 44. Polarization for cell electrodes at 400° C, 10 mA applied current. 76 ml/min of 0.3% SO_2, 3% O_2 in N_2.

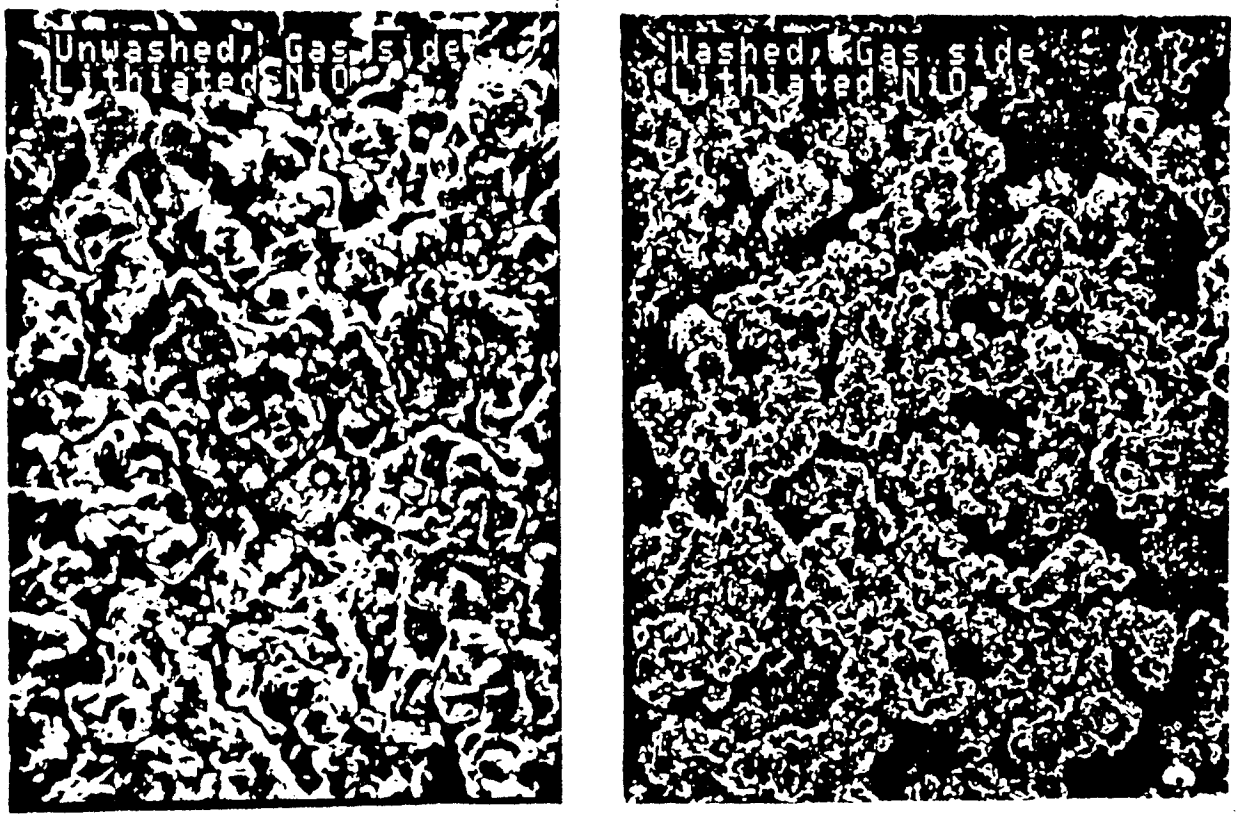

Figure 45. SEMs of ERC electrodes after use in the cell; unwashed (left) and washed (right). Both micrographs at same magnification.

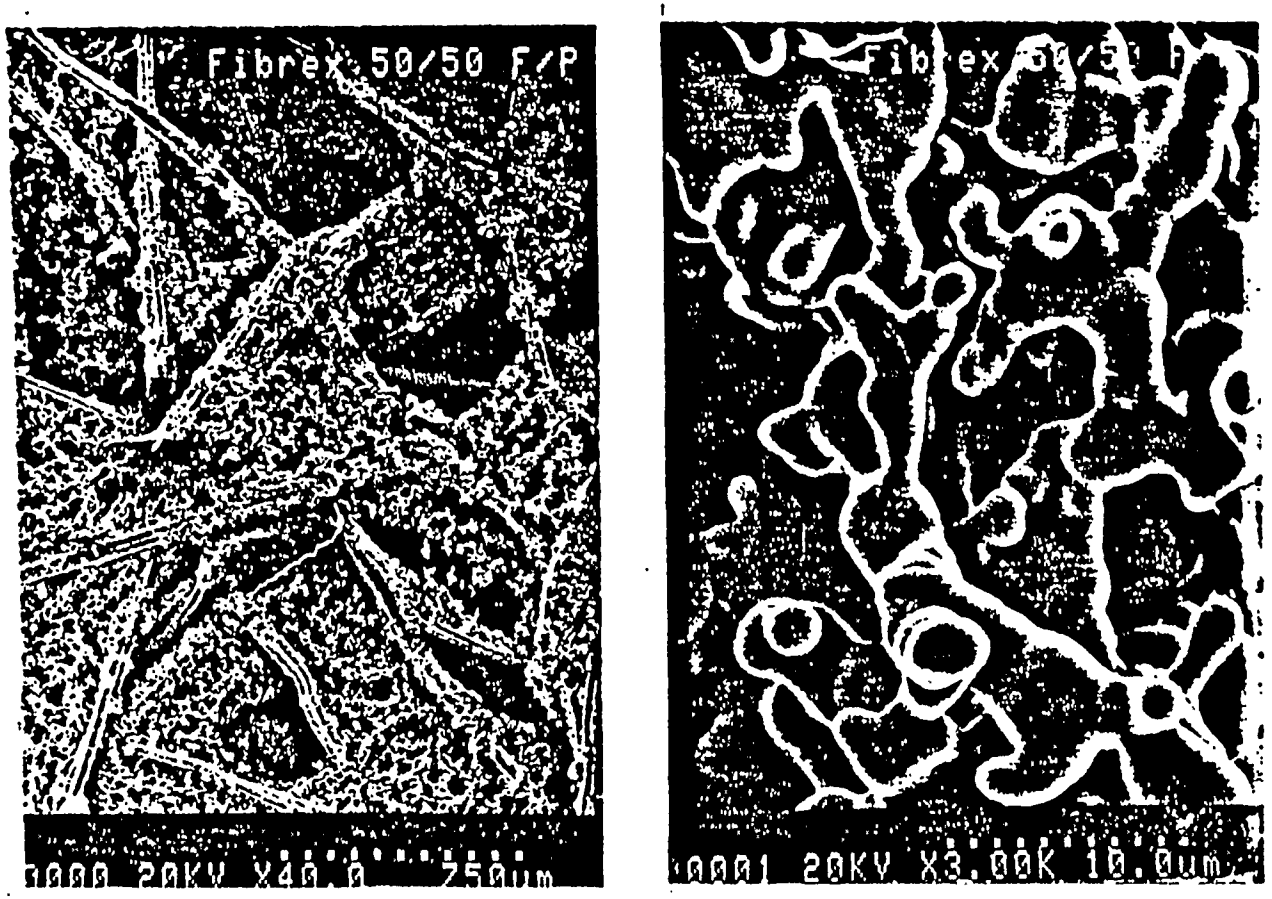

Figure 46. SEMs of Fibrex mesh, 50/50 : fiber/powder. Left, 40x; right, 3000x.

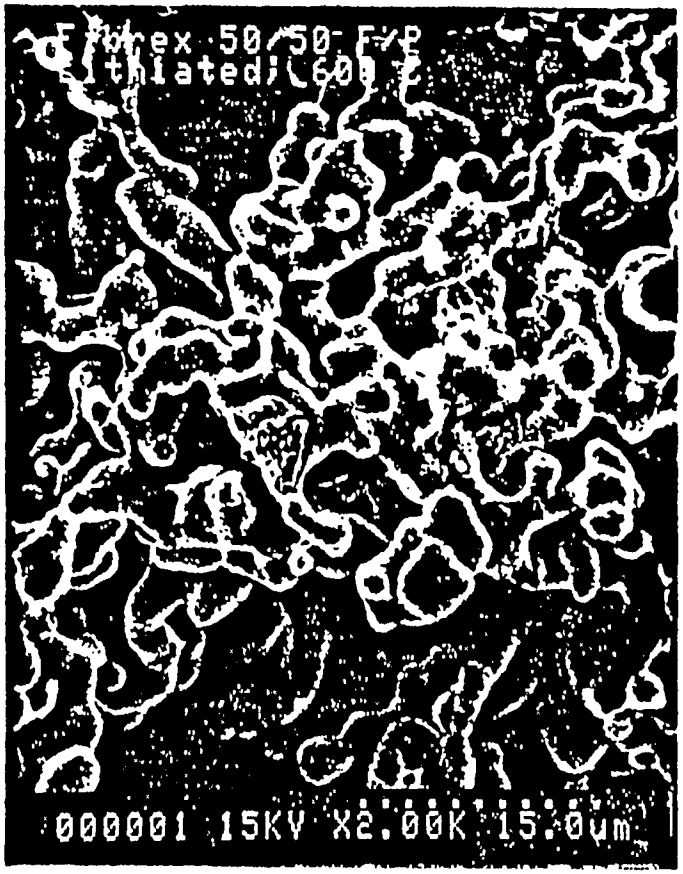

Figure 47. SEM of lithiated and oxidized 50/50 Fibrex Mesh.

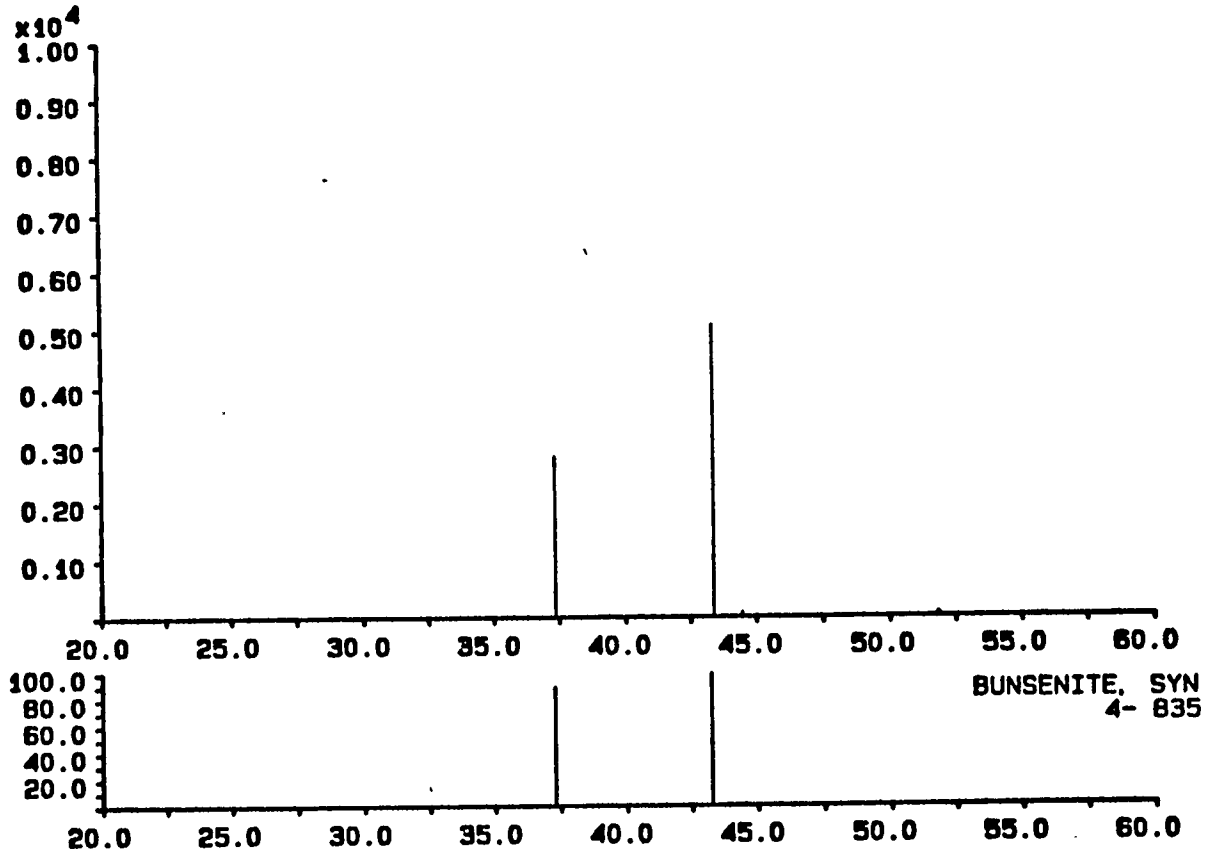

Figure 48: X-ray of oxidized and then lithiated ERC electrode.

Starting porosity of 86% (Fibrex)

January 13, 1993	Sample number-->	1	2	3	4	5	Averages	Standard Deviation
Measurement	Formula							
Dry Weight, g	D	1.466	1.674	1.945	1.152	2.045	1.656	0.324
Saturated Weight, g	M	2.644	2.967	3.585	2.159	3.698	3.011	0.577
Suspended Weight, g	S	1.274	1.454	1.661	1.013	1.792	1.439	0.277
		T(water)= 25C		density= 1 g/cc				
Exterior Volume, cc	V=M-S	1.370	1.513	1.924	1.146	1.906	1.572	0.304
Volume of open pores, cc	M-D	1.178	1.293	1.640	1.007	1.653	1.354	0.255
Volume of Impervious Portions, cc	D-S	0.192	0.220	0.284	0.139	0.253	0.218	0.050
Apparent Porosity, %	P=(M-D)/V*100	85.99%	85.46%	85.24%	87.87%	86.73%	86.26%	0.96%
Water Absorption, %	A=(M-D)/D*100	80.35%	77.24%	84.32%	87.41%	80.83%	82.03%	3.50%
Apparent Specific Gravity	T=D/(D-S)	7.635	7.609	6.849	8.288	8.083	7.693	0.496
Bulk Density, g/cc	B=D/V	1.070	1.106	1.011	1.005	1.073	1.053	0.039

Figure 49: Results of porosity standard on lithiated NiO electrodes (Fibrex).

Sample ID..... fibrex50 Filename..... DEN1.PRD
Instrument..... Autoscan 33 1X 0 - 33000 PSIG
Sample Description..... Fibrex 50/50; Lithiated 575C
Mercury Contact Angle.. 135.00 ° Mercury Surf Tension... 484.0 erg/cm
Sample Weight..... 0.8336 g Bulk Sample Volume..... 1.0000 cc
Minimum Delta Volume... 0.000 % FS

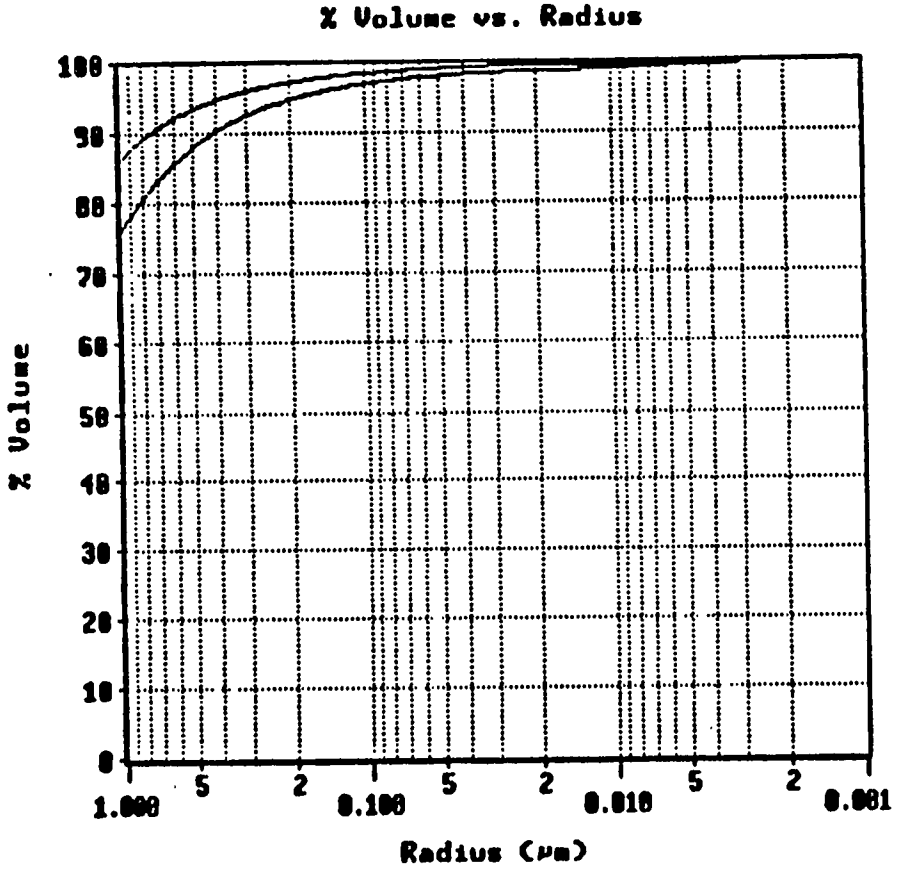

Figure 50. Mercury Porosimetry Curve for Lithiated and Oxidized Fibrex 50/50 mat.

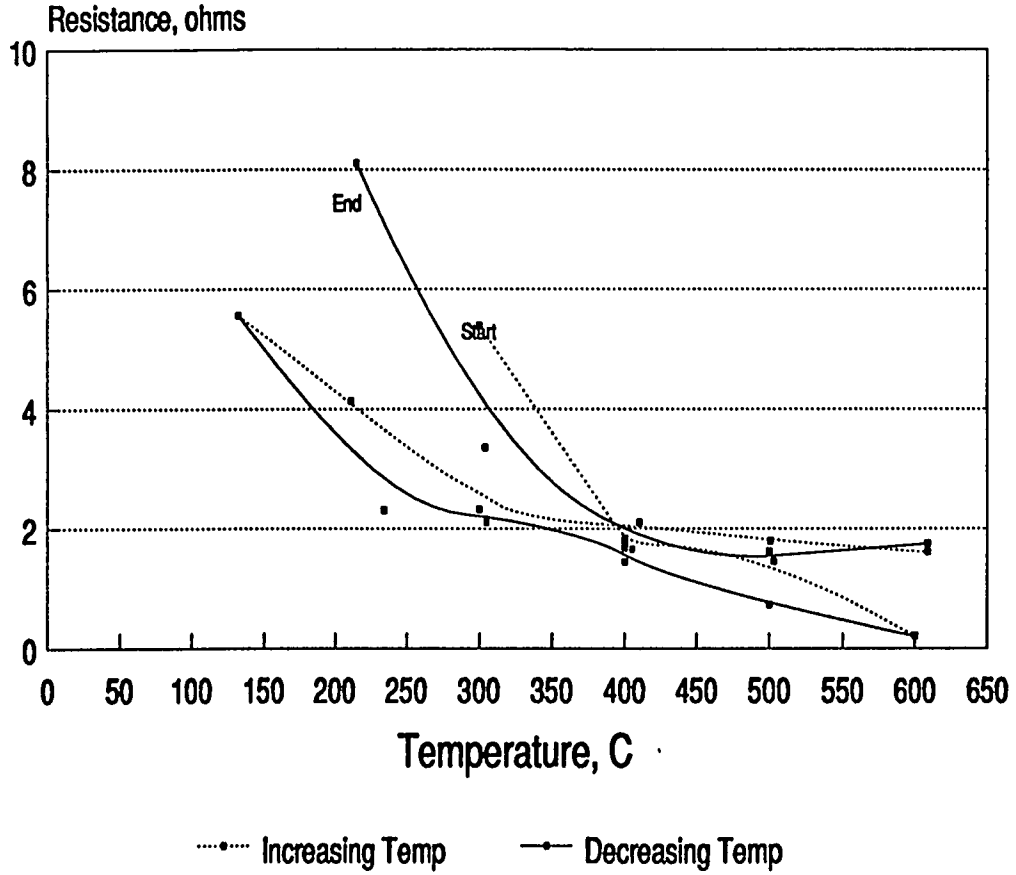

Figure 51: Cyclic resistance of a p-type semiconductor, LiNiO, with temperature.

Electrolyte Management

It is suspected that the 'in situ' introduction of electrolyte will lead to excellent gas seals in full scale testing of the SO_x removal cell. A search began for a method of management allowing the placement of electrolyte in the cell prior to binder burnout and cell heating. The presence of the electrolyte stabilizes the ceramic matrix, making it less susceptible to thermal and mechanical shock than an un-impregnated matrix.

The first attempt at this management was the tape casting of the electrolyte in a 78 vol% mixture with a polyvinyl binder. The result was an inhomogeneous mixture that yielded varying tapes. The slurry itself also presented difficulties, forming a jelly-like substance that was unmanageable. Only additional solvent allowed the mixture to be poured and cast.

A second attempt to tape cast the electrolyte in a 55.6 vol% mixture with the polyvinyl was made. The slurry was again unmanageable, and only the addition of 30 ml solvent (doubling the total volume) after 24 hours of milling allowed recovery of the slurry. The resulting tape cracked and adhered to the casting surface.

Attempts were then made to cold and hot press disks of pure electrolyte. The cold-press was carried out with 2.5 g electrolyte at 1050 psig for 5 minutes. The resulting disk was fragile and crumbled to the touch. Subsequent attempts at pressures of 1680 psig and 10 minutes produced the same results.

The hot press technique is somewhat arbitrary in this application. The presence of bisulfates in the pyrosulfate exposed to humidity greatly reduced the melting point; while bisulfates will melt and decompose to pyrosulfate upon heating, that melting is

not desirable in the hot pressing process. Hot pressing requires compression of the material at a point 10-15° C below its melting point. If that melting point is not well known, the procedure will tend to be ineffective. The melting point of the electrolyte was determined to be approximately 300-350° C, and a pressing temperature of 275° C was chosen. Three times, the die was baked in the oven for 5-10 minutes, and then pressed at 1050 psig for 1 minute. The resulting disk, while showing a slightly stronger mechanical strength than the cold pressed disk, still fell apart during handling.

A polymer was then used in conjunction with the electrolyte in the pressing. Polyethylene oxide was first milled with electrolyte for a minimum of 1/2 hour before placement between two cut aluminum foil circles in the pressing die. The die was then alternated between an oven and the press, for various numbers of cycles and at various temperatures. Pressing occurred at 1900 psig in all cases. This technique was tried with two different molecular weights of polyethylene oxide: 900,000 and 100,000. The results are shown in Table VII. Also shown in Table VII are the results of the use of hydroxyethyl cellulose, courtesy Union Carbide, in a combination with the electrolyte. The hydroxyethyl cellulose has been shown to burn out completely at a temperature of 350°C.

X-ray diffraction performed on an 80wt% electrolyte 20wt% hydroxyethyl cellulose disk after exposure to the atmosphere at 400° C showed the formation of multiple phases, with little to no potassium pyrosulfate detected. Reaction depletion of the pyrosulfate occurred. In addition, electrolyte was dissolved in an 80%/20% ethanol/toluene solution at 25° C. This solution is the solvent used in the polyvinyl

binder system discussed in earlier reports. The solution was dried with low heat, and filtered. X-ray diffraction, performed on the resulting solid, showed, again, a reaction had taken place. This result was expected, as pervious attempts to use the polyvinyl binder system had resulted in unusable material and membranes, confirming these methods did not represent the solution to in situ electrolyte introduction.

The most successful method of electrolyte introduction is to assemble the cell components minus the electrolyte, and raise the temperature under an air atmosphere. The matrix used was a tape cast ceramic. Organic components are burned away as the cell reaches its operating temperature of 400°C, leaving a porous ceramic matrix 50% porous by volume. Electrolyte is first brought to cell temperature, then introduced to the matrix through a hole cut in the upper housing for this express purpose. The molten electrolyte, by capillary action, is drawn into the porous ceramic, forming a viable membrane for use in testing. The hole used for electrolyte introduction is then sealed.

This method resulted in a practical cell, with a wet seal able to withstand a pressure of up to 1"H_2O both across the membrane and to the environment. All removal results utilized electrolyte introduction in this manner.

Table VII: Table of attempted electrolyte disk manufacture.

#	wt% Elect.	T(oven) (° C)	cycles	Oven Time	MW polymer	Mill Time (hr)	Results
6	66.7	155	3	7	900000	0.5	usable disk
7	81.4	100	3	10	900000	0.5	15% usable
9	66.7	165	3	10	900000	0.5	20% usable
10	50.0	155	3	15	900000	0.5	40% usable
11	33.3	162	6	16	900000	0.5	usable disk
12	66.7	156	1	7	100000	1.0	25% usable
13	66.0	158	2	10	100000	1.0	usable disk
15	85.7	158	2	10	100000	1.0	usable disk
16	80.0	158	2	10	100000	1.0	90% usable
17	75.0	158	2	10	100000	1.0	usable disk
18	85.7	158	2	10	100000	2.0	10% usable
19	75.0	158	2	10	900000	2.67	70% usable, but brittle
20 *	69.4	------	1	---	30000	1.0	60% usable
21 *	71.4	------	1	---	30000	1.0	85% usable
22 *	62.5	------	1	---	300	1.0	90% usable
23	85.7	158	3	20	100000	1.0	75% usable
24 *	55.5	------	1	---	300	1.0	90-95% usable
25 *	69.4	------	1	---	300	1.0	70% usable

* = denotes the use of hydroxyethyl cellulose, courtesy Union Carbide Corporation, which was cold-pressed.

All others use polyethylene oxide.

Electrolyte Experiments

Before any type of model for electrode wetting can be developed, the transport properties of the molten electrolyte must be known. While much data is available for potassium sulfate, little is known about potassium pyrosulfate, and even less about a mixture of potassium pyrosulfate and vanadium pentoxide. A simple experiment was performed to determine the density of the molten salt at 400° C.

A Pyrex graduated cylinder was used to determine the density. The coefficient of linear thermal expansion for Pyrex is listed as 0.033×10^{-8} [33] up to 300° C. The expansion of the cylinder due to the increase in temperature was therefore assumed negligible. The cylinder was loaded with a known weight of electrolyte, covered to maintain a constant SO_3 partial pressure, and heated. Readings were taken over a 4 hour period. The loss of weight was found to be 0.083 g ±.005 g possibly due to SO_3 formation or vaporization of any water present on the surface of the cylinder. This small loss was considered negligible. The beginning and end weights were averaged, and the density at 400° C was calculated as 1.997 g/ml ±0.05 g/ml. Error in this experiment may result from an inaccurate reading, or solidification of the molten salt when the oven was open to read the height. Solid density of the electrolyte is predicted to be 2.346 g/ml when using a correlation suggested by Prausnitz[34].

An attempt was then made to calculate the surface tension of the electrolyte. Lovering[35] has suggested Jaeger's[36] maximum bubble method as an excellent technique with which to measure the surface tension of a molten salt. The method requires the

$$p = \rho g h + \frac{2\gamma}{r} \qquad (59)$$

ability to measure the pressure required to force one N_2 bubble out of an opening at a known depth. This pressure is assumed to be due to the depth of the liquid and the force required to overcome the surface tension of the liquid, forming a bubble. The equation used is shown as Equation (59), where p=pressure, h=depth of immersion for tip of capillary, r=radius of the capillary opening, g=gravitational constant, ρ=density of the melt, and γ=surface tension. An apparatus was then developed for the experiment (see Figure 52), and a mercury manometer was used to measure the pressure difference.

The result is encouraging, although the range is large. The manometer read only a 6 mmHg difference, providing the largest relative source of error, and was treated as such in the analysis. The final value for surface tension from the maximum bubble pressure method was 138.8 dynes/cm ± 33.4 dynes/cm.

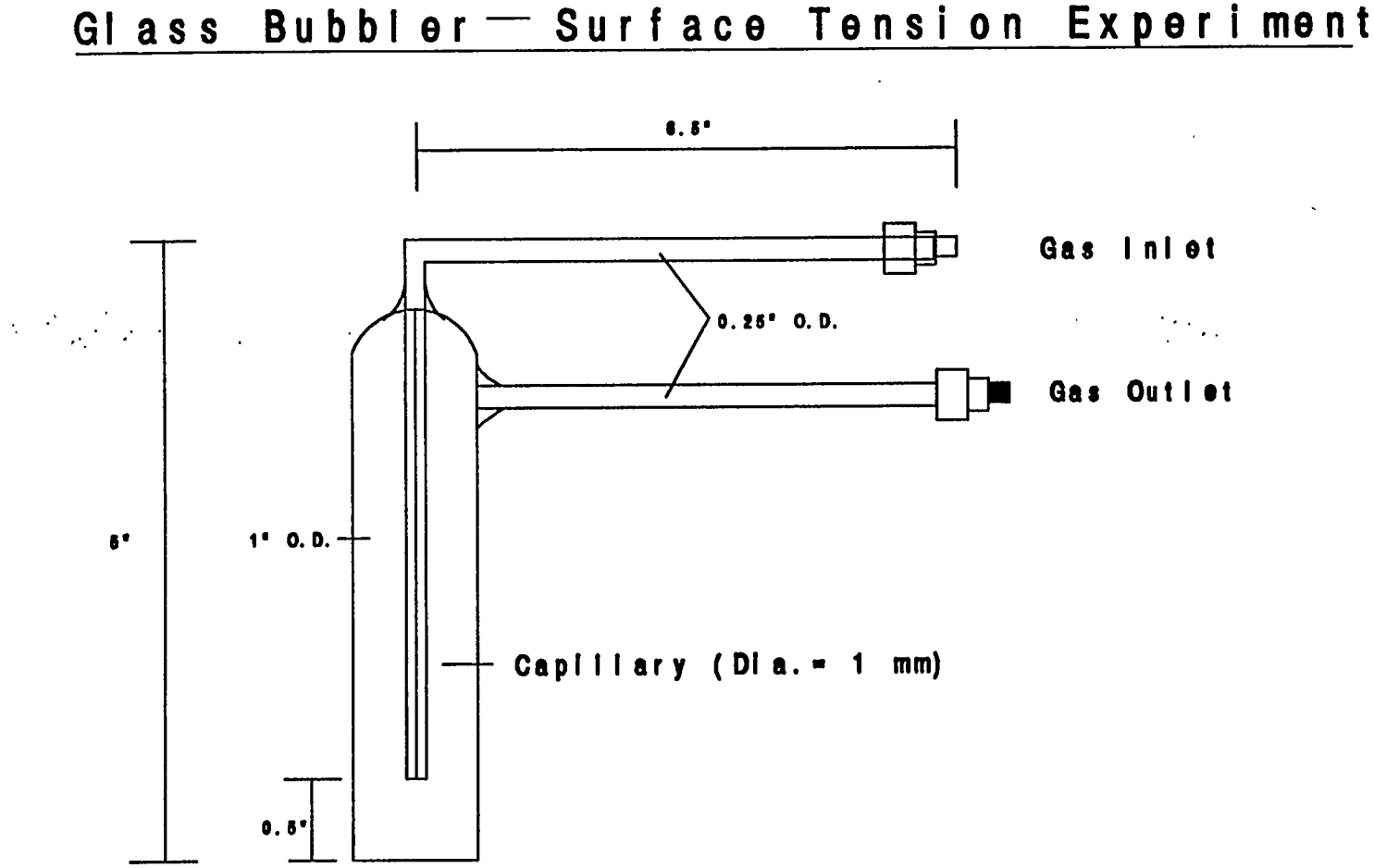

Figure 52: Capillary apparatus used in an attempt to determine the surface tension of molten electrolyte.

Matrix

General analysis was conducted on several candidate matrix materials. These included a magnesium oxide (MgO), zeolites, two borosilicate glass preparations, silicon carbide, three silicon nitride materials, crystalline and amorphous silica (SiO_2), and zirconia (ZrO_2).

Magnesium Oxide

Work initially used hot pressed MgO as a matrix material Franke[26] found that the MgO was actually a matrix precursor, with the true matrix material being formed through reaction with the electrolyte:

$$2MgO + 2K_2S_2O_7 \rightarrow K_2Mg_2(SO_4)_3 + K_2SO_4 \qquad (60)$$

so that the $K_2Mg_2(SO_4)_3$ became the true matrix material, and the resulting potassium sulfate dissolved in excess electrolyte.

Zeolite

Zeolites were screened via a preliminary test. The zeolites were dried in a vacuum desiccator for 48 hours, mixed with a quantity of uniform electrolyte (a single preparation of 5wt%V_2O_5 in $K_2S_2O_7$ heated to 400°C) and placed in sealed Pyrex tubes seen in Table VIII.

As the blends were heated, the electrolyte melted and penetrated the pores of the zeolites. Silicalite (ZSM-5) had wet spots of electrolyte throughout while other zeolites absorbed all of the molten salt. The difference in behavior was attributed to the polar nature of the zeolite. 13X, 4A, and 5A have lo SiO_2:Al_2O_3 ratios, making them highly polar. the nature of the matrix attracts the electrolyte and permits absorption in the pores. Silicalite, with a ration of 280, was non-polar and thus had reduced absorption.

Borosilicate

The borosilicate glass materials were prepared by wet milling <325 mesh (<44 microns) glass for 6 or 7 days.

Several tapes were cast from a blend of 45 volume percent (^{V}/o) glass in vinyl butyryl binder (Metoramic B73305). Varying results were found upon burnout, depending on drying conditions. Some tapes dried too rapidly, causing minor mud cracks on the surface. These mud cracks caused cracking of the membranes upon heating to T > 450° C. When drying conditions were better controlled, no cracking resulted in the membrane, allowing complete wetting of the matrix with electrolyte.

Zirconia

Two full cell tests were conducted during this quarter with Zircar fabrics. The fabric is made from yttira-stabilized (8 ^{W}/o Y_2O_3) zirconia, in either knitted or woven form. Since these materials worked well in the H_2S removal process, preventing gas crossover and retaining sufficient electrolyte, they were tested here.

During full cell testing, performance of the fabric decayed over time. Cell resistance increased, to the point of prohibiting passage of current. Post-mortem analysis showed the fabric to react with the $K_2S_2O_7$ electrolyte, leaving the electrolyte phase enriched in K_2SO_4. The remaining membrane was water soluble, confirming the reaction of the fabric, with the formation of water soluble zirconyl sulfates. These fabrics were dismissed as viable membrane matrices.

Silica

Amorphous SiO_2 was tested, pressed by a new leach technique developed at Georgia Tech. The chemical stability of this material needed to be tested, as well as the ability of the electrolyte to saturate the matrix, as crystalline silica is known to react with pyrosulfate. To this end, two samples of different manufacture were exposed to 90wt% $K_2S_2O_7$/ 10wt% V_2O_5 at 400° C in Pyrex petri dishes for 48 hours in air. The results were then analyzed using SEM and X-ray diffraction.

The first sample (10-90) surface was non-discernable (see Figure 54). The counterpart to this sample, which was tested as described above, wet throughout with electrolyte. The SEM analysis, however, only picked up what may be frozen electrolyte on the surface, as seen in Figure 55.

The second sample analyzed (3070) was of greater porosity, and apparently greater pore size than the first. The most striking feature of the surface is the rod-like formations. This matrix material easily saturated with electrolyte at a much greater

speed than the 10-90 sample. The resulting SEM of the saturated material is shown below.

The exposed samples were cooled, and x-rayed without washing (see Figure 56). Potassium pyrosulfate/vanadium pentoxide peaks were seen. The amorphous peak seen in the pure sample was also present. An extensive analysis of the possible sulfur and vanadia species failed to show any new phases due to reaction. This result indicates a chemical inertness of this proposed matrix material, but does not verify any electrochemical stability, as this material is very similar in structure and properties to the previously rejected ZrO_2.

DuPont's LUDOX AS-40 silica particle suspension was investigated also. When removed from suspension, the large agglomerates of silica formed, which were ground. However these particles did not wet with the electrolyte. Other silicas from Degussa showed the same inability to wet. Crystalline silica has been shown by other researchers to react with sulfate ions.[37]

Silicon Nitride/Silicon Carbide

One silicon carbide samples and two silicon nitride samples were obtained courtesy Phillips Petroleum, and one silicon nitride sample was obtained courtesy Oak Ridge National Laboratories. Particle analysis of each sample is shown in Table IX.

Samples of each material were subjected to chemical testing to determine chemical stability before use as a matrix material. Each material, seen in Table X, was exposed

to $K_2S_2O_7$ for 7 days at 400°C. These tests identified several stable chemical matrix materials for further study.

Several matrix materials were then used in full cell studies to evaluate relative polarizations, and identify the most favorable material for extended testing. Evaluation of the overpotential seen in Figure 57 suggests that of those materials tested, Si_3N_4 provided the most favorable polarizations.

Manufacture

Three methods of matrix manufacture were attempted, with varying success:

(1) Hot/Cold Pressing and Sintering

(2) Slip casting

(3) Tape casting

Pressing and Sintering

Dry powder was packed uniformly into a die of 3" diameter, to thicknesses of 1mm to 1.5mm. The die was then taken to a hydraulic press, with a applied pressure of 1132 psig. The resulting disk is then transferred to a firing plate, covered, and placed in an oven with a slow temperature ramping to 1150° C, held at that temperature for a period of time, and slowly brought back down to room temperature.

The first attempt resulted in an amalgamation of alumina and silicon nitride. The silicon nitride disk, after pressing, was fired on an alumina firing plate in an oxygen atmosphere. An unidentified liquid phase formed, resulting in warping of the disk, and the general defacing of the alumina firing plate,[38] and yielded a highly densified new phase, seen in Figure 58. Such a phase is not desired. Although it may be inert to the system, the ceramic will not allow impregnation by the electrolyte to any appreciable extent. Interconnecting microchannels are necessary for migration of sulfate from cathode to anode where it can be oxidized.It was suggested[39]that the firing be done in an inert atmosphere of nitrogen, and on a surface of either silicon nitride or silicon boride. In addition, a solid-phase diagram was prepared, shown in Figure 59, to ensure the material obtained from the process was the material desired.

A reaction-bonded plate of silicon nitride was obtained from Norton Industrial Ceramics. A test disk of 1" diameter was pressed and fired under high purity nitrogen (Holox, 99.97 purity), with excellent results. The plate obtained, however, was not large enough to support a 3" diameter disk.

Discussion with Paul Kohl, Professor, Georgia Institute of Technology, revealed that the chemical vapor deposition (CVD) of pure Si_3N_4 onto Si wafers was common technology. Four such wafers were prepared by Martin Ceiler, Chemical Engineering, Georgia Institute of Technology, with ~9000Å of pure silicon nitride deposited onto the surface.

A 3" diameter disk was pressed at a pressure of 1132 psig, and fired under high purity nitrogen. The resulting disk was found to be of sufficient mechanical strength,

The first attempt resulted in an amalgamation of alumina and silicon nitride. The silicon nitride disk, after pressing, was fired on an alumina firing plate in an oxygen atmosphere. An unidentified liquid phase formed, resulting in warping of the disk, and the general defacing of the alumina firing plate,[38] and yielded a highly densified new phase, seen in Figure 58. Such a phase is not desired. Although it may be inert to the system, the ceramic will not allow impregnation by the electrolyte to any appreciable extent. Interconnecting microchannels are necessary for migration of sulfate from cathode to anode where it can be oxidized.It was suggested[39]that the firing be done in an inert atmosphere of nitrogen, and on a surface of either silicon nitride or silicon boride. In addition, a solid-phase diagram was prepared, shown in Figure 59, to ensure the material obtained from the process was the material desired.

A reaction-bonded plate of silicon nitride was obtained from Norton Industrial Ceramics. A test disk of 1" diameter was pressed and fired under high purity nitrogen (Holox, 99.97 purity), with excellent results. The plate obtained, however, was not large enough to support a 3" diameter disk.

Discussion with Paul Kohl, Professor, Georgia Institute of Technology, revealed that the chemical vapor deposition (CVD) of pure Si_3N_4 onto Si wafers was common technology. Four such wafers were prepared by Martin Ceiler, Chemical Engineering, Georgia Institute of Technology, with ~9000Å of pure silicon nitride deposited onto the surface.

A 3" diameter disk was pressed at a pressure of 1132 psig, and fired under high purity nitrogen. The resulting disk was found to be of sufficient mechanical strength,

although this was not explicitly tested except in handling. It is known that the sintering of pure silicon nitride results in a final porosity of approximately 65% at a temperature of up to 2073 K[40]. The final porosity of the sintered membrane was estimated to be 50%, with incomplete sintering at the low firing temperatures.

The disk was used in a full scale run. Cracking was heard upon cell assembly, but the test proceeded in the hope that the electrodes had broken, leaving the membrane intact. The introduction of electrolyte into the matrix was an unusually slow process, and consequentially, excess electrolyte was added, flooding the electrodes. The concern that, in a time period of 1 hour, the matrix had not been completely wetted was found to unjustified post-mortem, as the small capillaries seem to simply take a longer amount of time to properly wet. The additional electrolyte plugged the outlet tubes. They were immediately cleaned, but gas-crossover began in the interim. The disk, upon examination, was noted to have a few hairline fractures, possibly due to assembly rather than post-mortem examination.

Slip Casting

Slip casting of the silicon nitride was attempted. Slip casting, is the mixing of the ceramic into a slurry, and pouring the slurry into a mold. The solvent is drawn off by the mold, leaving the resulting ceramic in the desired shape. Thickness is controlled by the solvent/ceramic ratio, speed of casting, and relative solvent humidity conditions. The casting solution may contain only the solvent, or some mixture of solvent, binder,

surfactant, or dispersant, all of which will affect the casting ability and resulting ceramic piece.

The attempt was made, again using the Phillips Petroleum silicon nitride, in conjunction with water as the solvent, and using Darvan C, courtesy Konrad C. Reiger of the R.T. Vanderbuilt Company, Inc., as the dispersant, to slip cast a membrane. Darvan C has a low ash content on burnout, and has shown low foaming in Vanderbuilt tests.

A slurry was mixed in a beaker, with DI-H_2O (18.3 Ω-cm), Darvan C, and silicon nitride in a, respectively, 48.3 wt%/0.3 wt%/51.4 wt% mixture, for a total of 20.570g. Mixture viscosity was visually estimated as correct. The slurry was then poured into the full cell housings, with electrodes in place, and the top housing was pressed onto the slurry top to form a membrane of a thickness of approximately 1.5mm. Unfortunately, the electrodes and housings were dry, and the water was quickly absorbed into the electrodes, setting the slurry in a less-than-ideal configuration. No seal was ever developed while used in full cell tests with an estimated amount of electrolyte, and the cell test was terminated. The resulting membrane utilizing this method was determined to be too thick in comparison to tape casting and pressing methods, as well as difficult to implement in method.

Tape Casting

The casting procedure used utilizes a polyvinyl butyryl binder, in a benzene/toluene solvent. This prepared mixture, including some dispersants and

surfactants, was obtained from Metoramic Sciences. The binder (see Table XI for characteristics of binders used) is added in an appropriate quantity, such that, after burnout, the resulting ceramic and ash left will occupy 50% by volume of the apparent volume of the ceramic disk.

After binder mixing, additional solvent and surfactant is added as needed to keep the solution at an appropriate viscosity. The slurry is mixed in an alumina ball mill, and is sonicated prior to casting.

Casting takes place on an appropriate surface, either glass, galvanized steel, or teflon, depending on the surfactant and dispersants used in formulation. Spacers are used so that a doctor blade may be drawn across the surface at a height of 1 mm relative to the surface. The mixture is poured onto the surface, and the doctor blade is drawn across to produce a uniform height. The wet tape is then covered completely to slow down the evaporation of the solvent, allowing the tape to dry uniformly, without cracking or undue stress. Drying is done overnight, or as required.

The resulting 0.30mm thick (corresponding to approximately 70% solvent by volume i the original slurry) green tape is then removed from the substrate, and cut to the proper form. It can be pressed or combined with other tapes as desired, as it is extremely pliable at this point. As the tape is subjected to higher and higher temperatures, as in full cell tests, the organics volatilize with oxygen, and burn out completely by 380° C, according to a Metoramic Sciences TGA, leaving only a small amount of ash. The resulting ceramic matrix may then be impregnated with electrolyte.

Various problems have arisen in the application of this much-desired process. The use of B (SiC) was attempted with little success except at low (11% ceramic) loading levels of the tape. The results of various attempts can be seen in Table XII. The one B membrane that did cast (#3, Table XII) was used, and was shown to have inadequate ceramic volume to maintain the matrix. A higher volume percentage ceramic is needed.

Another problem arose when attempting to cast C (Si_3N_4) due to the small particle size, with such a large surface area (80 m^2/g). There is a constant problem of surface wetting by the polymer due to the large surface area. The natural alleviation of this problem is the addition of binder to the system. This will result, however, in the reduction of volume percent ceramic, which leads, as previously discussed, to a mechanically intolerable system.

Additional solvent is then the possible solution. The result, however, tends to choose one of two avenues: the large amount of solvent evaporation leads to a cracked green tape; or the mixture is not homogenous, with viscous and less-viscous phases present, resulting in an non-uniform green tape. Neither of these two results is at all desirable.

Additional surfactant has been tried in an attempt to reduce the amount of solvent required to obtain a homogenous mixture. This carries its own problems: solvent evaporation will be slowed down at the surface, as the surfactant increasingly inhibits easy solvent evaporation as it travels to the surface with the solvent and accumulates due to its lower vapor pressure. Again, internal stress may result, as solvent is trapped inside the drying tape, resulting in cracking of the tape.

Solutions to this problem were discussed with Metoramic Sciences[41]. Among the solutions discussed is the variation of solvents to from just ethanol and toluene to include possibly acetone or MEK. Some of these may not be feasible, however, as the rate of evaporation would increase in some cases, possibly leading to cracking. Additional surfactants were also been discussed, including acetates, high carbon acids, and possible phosphoric acid, along with some amides, aminos, and polyesters.

Tape cast C and F, however, have shown excellent results due in part to their low surface area to weight ratios. Figure 60 shows the results of loading levels of 50 vol% F, after the binder is burned out. It can easily be seen that there exist interconnecting channels into which electrolyte can be impregnated. The picture does exhibit surface roughness, a sign that the particles are not as structured as might be desired. This may lead to lower capillary force at the surface, and possible loss of electrolyte from the matrix, neither of which is desired. Scrap was tested in air at 400° C to insure that the structure did in fact wet properly, and capillary action would carry the electrolyte through the ceramic structure.

To correct this problem, the tape is pressed prior to use in full cell testing. This pressing will tend to remove any trapped gases, and order the particles, especially at the surface. The results of such pressing can be seen in Figure 53. The surface of the membrane is much more uniform than the unpressed membrane. In addition, average pore size was qualitatively reduced, leaving smaller pores. Testing showed this matrix would saturate with molten electrolyte, though not as quickly as matrices with larger pores.

Membranes used in full cell testing generally consisted of two tapes, cut to appropriate size, and pressed together at approximately 9000 psig. These tapes were then placed in the cell under O_2 flow and allowed to burn out at 350° C. Electrolyte was introduced to the cell at this point, and the cell was sealed. Thickness of the membranes used averaged about 0.55mm.

Table VIII: Zeolite Mixture Test Samples. Electrolyte was 5wt%V_2O_5 in $K_2S_2O_7$.

Sample #	Zeolite	Mix Composition
1	13X	1.0000g 13X 0.9968g electrolyte
2	Silicalite	0.9633g Silicalite 0.9583g electrolyte
3	4A	0.9564g 4A 1.0007g electrolyte
4	5A	0.9564g 5A 1.0038g electrolyte
Control	-	0.9903g electrolyte

Table IX: Si_3N_4/SiC powder characteristics.

Binders									
Name	SC-P		SN-R		SN-P		Oak Ridge National Laboratory		
Manufacturer	Phillips Petroleum		Phillips Petroleum		Phillips Petroleum		UBE Ind., Ltd.		
Designation	B		C		D		F		
Formula	SiC		Si_3N_4		Si_3N_4		Si_3N_4		
surface area, m^2/g	10		90		5		10.9		
Particle size, µm	0.3		0.2		2.0		0.5		
Composition, wt%									
Si	69.0		58.5		59.0				
N			32.0		37.5		>38.0		
O	2.0		7.7		2.5		1.29		
C	29.0		1.8		1.0		<0.2		
trace, ppm	<400		<400		<400		<300		
Phase Composition	Beta >99%		Amorphous		Alpha >95%		Alpha >95%		

Table X: Results of chemical stability testing of candidate matrix materials.

Material	Result
Control	Decomposed to K_2SO_4
MgO	Reacted to $K_2Mg_2(SO_4)_3$
borosilicate glass	Amorphous - inconclusive
Silicalite	New phase - unidentified
SiO_2	Amorphous - inconclusive
SiC (B)	Stable
Si_3N_4 (C)	Stable
Si_3N_4 (D)	Stable